Journal of Alloys and Compounds 517 (2012) 186–191

Contents lists available at SciVerse ScienceDirect

Journal of Alloys and Compounds

journal homepage: www.elsevier.com/locate/jallcom

Synthesis and electrochemical properties of $LiMn_2O_4$ and $LiCoO_2$-coated $LiMn_2O_4$ cathode materials

Hong-En Wang[a,b], Dong Qian[a,b,*], Zhou-guang Lu[a], Yong-kun Li[a]

[a] College of Chemistry and Chemical Engineering, Central South University, Changsha 410083, PR China
[b] State Key Laboratory of Powder Metallurgy, Changsha 410083, PR China

ARTICLE INFO

Article history:
Received 7 August 2009
Received in revised form
18 December 2011
Accepted 19 December 2011
Available online 26 December 2011

Keywords:
Oxide materials
Electrode materials
Chemical synthesis

ABSTRACT

The synthesis of spinel $LiMn_2O_4$ material by a spherical MnO_2 precursor route is reported in this paper. Hydrothermal and solid-state reactions were adopted to investigate the effects of synthetic methods on the morphologies and electrochemical characteristics of the $LiMn_2O_4$ products, respectively. $LiCoO_2$-coated $LiMn_2O_4$ microspheres were also prepared by a sol–gel route based on the as-prepared $LiMn_2O_4$ microspheres. The products were characterized by powder X-ray diffraction (XRD), scanning electron microscopy (SEM), energy-dispersive X-ray spectrum (EDX), and inductively-coupled plasma emission spectrograph (ICP-ES). The results show that $LiMn_2O_4$ octahedrons can be obtained under hydrothermal conditions while $LiMn_2O_4$ microspheres can be prepared by the solid-state reaction. Electrochemical characterization reveals that the resulting $LiMn_2O_4$ microspheres and $LiCoO_2$-coated $LiMn_2O_4$ microspheres display much better cycling properties than those of $LiMn_2O_4$ octahedrons.

1. Introduction

In recent years, spinel $LiMn_2O_4$ has been intensively investigated as a promising candidate for cathode materials of lithium-ion batteries (LIBs) due to its low cost, non-toxicity, environmental friendliness, easy preparation, excellent voltage profile, and operating safety characteristics [1,2]. For the realization of practical industrial application, it is important to produce $LiMn_2O_4$ powders with excellent capacity and cycle stability. It is known that the electrochemical properties of the cathode are strongly dependent on its physical characteristics such as the particle size and morphology [3,4], crystallinity [5] and composition [6]. A lot of synthetic methods have been successfully developed to prepare spinel $LiMn_2O_4$ materials with different morphologies, grain sizes, granularity distribution, crystallinity, and composition. The most common route for the preparation of spinel $LiMn_2O_4$ is based on the solid-state reaction [7,8]. This process is simple and usually requires mechanical mixing, grinding, and repeating calcinations at high temperatures. In addition, several other chemical processes such as co-precipitation [9], emulsion drying [10], sol–gel [11], Pechini process [12], and hydrothermal [13,14] have also been developed to produce spinel $LiMn_2O_4$ powders.

However, pure spinel $LiMn_2O_4$ usually suffers a relatively poor cycle stability and an insufficient rate capability. It is believed that the capacity fading of $LiMn_2O_4$ is mainly attributed to three factors: (i) the Jahn–Teller distortion caused by the presence of Mn^{3+} Jahn–Teller ions [15], (ii) the dissolution of Mn ions into electrolyte [16], and (iii) the decomposition of electrolyte solution during the charge–discharge process [17]. To solve this problem, on the one hand, several research groups have tried to improve the cycling properties of $LiMn_2O_4$ by doping various metal elements such as Co, Cr, Ni, Fe, Ti, Zn, and Nd [18–22]. On the other hand, surface modification of $LiMn_2O_4$ with various oxides such as $LiCoO_2$ [23,24], Al_2O_3 [25], TiO_2 [26], ZnO [27,28], $AlPO_4$ [29], CeO_2 [30], $Li_4Ti_5O_{12}$ [31], ZrO_2 [32], and Li_2O–$2B_2O_3$ [33] has been widely undertaken.

Recently, it has been reported that spherical electrode materials can possess high discharge capacity and good capacity retention because they can have higher energy density and reduce the contact interface of electrode with the electrolyte, resulting in the improvement of cycling properties. He et al. [34] synthesized spherical $MnCO_3$ by a controlled crystallization method, and then obtained spherical $LiMn_2O_4$ material by a solid-state reaction between the $MnCO_3$ precursors and lithium salts. Sun et al. [35,36] prepared spherical $[Ni_{0.4}Co_{0.2}Mn_{0.4}]_3O_4$ and $Li[Ni_{0.8}Co_{0.1}Mn_{0.1}]O_2/Li[Ni_{0.8}Co_{0.2}]O_2$ materials for lithium secondary batteries by an ultrasonic spray pyrolysis and a co-precipitation process, respectively. Taniguchi et al. [37] synthesized spherical $LiMn_2O_4$ microparticles by a combination of spray pyrolysis and drying method. In addition, $LiMn_2O_4$ nanorods with fine electrochemical properties have also been prepared by

* Corresponding author at: College of Chemistry and Chemical Engineering, Central South University, Changsha 410083, PR China. Tel.: +86 731 88879616; fax: +86 731 88879616.
E-mail address: qiandong6@vip.sina.com (D. Qian).

0925-8388/$ – see front matter © 2011 Elsevier B.V. All rights reserved.
doi:10.1016/j.jallcom.2011.12.079

solid-state reactions with α-MnO_2 [38] and β-MnO_2 [39] as precursors, respectively.

In our previous paper [40], we synthesized spherical MnO_2 particles, and further made a simple attempt to produce $LiMn_2O_4$ microspheres with the prepared MnO_2 spheres as precursors. In this paper, we report the preparation of spinel $LiMn_2O_4$ by a spherical MnO_2 precursor route. Hydrothermal and solid-state reactions were adopted to synthesize spinel $LiMn_2O_4$ materials, respectively. The effects of the two different synthetic routes on the morphologies and electrochemical properties of $LiMn_2O_4$ were investigated. Moreover, $LiCoO_2$-coated $LiMn_2O_4$ microspheres were prepared based on the as-synthesized $LiMn_2O_4$ microspheres by a sol–gel route.

2. Experimental

All the chemical reagents were of analytically pure grade and used without any further purification.

2.1. Synthesis of MnO_2 spherical precursors

The synthesis of MnO_2 spherical precursors was referred to our previous report [41] with some modifications. In a typical procedure, 0.05 mol of $MnSO_4{\cdot}H_2O$ and equal amount of $K_2S_2O_8$ were dissolved in 1000 ml of distilled water to form a clear and colorless solution, followed by the addition of 5 ml of concentrated sulfuric acid. The resulting transparent solution was placed in a 40 °C water bath for 48 h. After the reaction was finished, the black precipitates were filtered off, washed with distilled water until the absence of SO_4^{2-}, which was tested by a diluted $Ba(NO_3)_2$ aqueous solution, and then rinsed with ethanol for several times. The resulting samples were dried in a vacuum oven at 120 °C for 6 h and then employed for the synthesis of $LiMn_2O_4$ samples.

2.2. Syntheses of $LiMn_2O_4$ samples by hydrothermal and solid-state reaction, respectively

For the preparation of $LiMn_2O_4$ samples, two different methods, namely, hydrothermal and solid-state reactions were employed, respectively.

For the hydrothermal synthesis of $LiMn_2O_4$, 0.87 g of the as-prepared MnO_2 spherical precursors and 0.42 g of $LiOH{\cdot}H_2O$ were placed in a 36 ml Teflon-lined autoclave, followed by the addition of 24 ml of distilled water. After stirring the mixture for 15 min, the autoclave was sealed, heated in an oven at 180 °C for 20 h, and then allowed to be cooled to room temperature naturally. The black precipitates were collected by filtration, washed with distilled water and absolute ethanol for several times, and then dried in a vacuum oven at 120 °C for 6 h.

For the solid-state synthesis of $LiMn_2O_4$, $LiOH{\cdot}H_2O$ and the as-prepared MnO_2 spherical precursors with an appropriate molar ratio of 1.05:2 were mixed and manually ground in an agate mortar for about 10 min. Then the mixture was pre-calcined in a muffle at 320 °C for 12 h, calcined at 750 °C for 8 h, and then cooled to room temperature naturally to give $LiMn_2O_4$ product.

2.3. Synthesis of $LiCoO_2$-coated $LiMn_2O_4$ by a sol–gel route

$LiCoO_2$-coated $LiMn_2O_4$ was synthesized by a sol–gel method. Firstly, citric acid was dissolved in ethylene glycol with a molar ratio of 1:4 at 80 °C to form a clear and transparent solution. Then, stoichiometric amounts of lithium acetate ($Li(CH_3COO){\cdot}2H_2O$) and cobalt acetate ($Co(CH_3COO)_2{\cdot}4H_2O$) with a cationic ratio of Li:Co of 1:1 were dissolved into the above solution and continuously stirred at 80 °C until the molar concentration of the solution was condensed to 1 M. Next, an appropriate amount of $LiMn_2O_4$ microspheres synthesized by the solid-state reaction described above with a molar ratio of Co:Mn of 1:20 was added to the solution along with stirring to form a sol. The sol was further transferred into a vacuum oven and dried at 120 °C to obtain a dry gel. Finally, the dry gel was placed in a muffle and pre-heated at 320 °C for 24 h, followed by calcining at 750 °C for 5 h. After cooling to room temperature naturally, $LiCoO_2$-coated $LiMn_2O_4$ microspheres would be obtained as a result.

2.4. Characterization of the as-prepared MnO_2, $LiMn_2O_4$, and $LiCoO_2$-coated $LiMn_2O_4$ samples

Crystal structures of the prepared samples were identified with powder X-ray diffraction (XRD) taken on a Rigaku-D-Max rA 12 kW Diffractometer (Cu Kα radiation, λ = 1.54056 Å) at an operation voltage and current of 40 kV and 300 mA, respectively. Scanning electron micrograph (SEM) and energy-dispersive X-ray analysis (EDX) were performed on a JEOL JSM-6360LV scanning electron microscope equipped with an EDX-GENESIS 60S. Chemical composition of the prepared $LiCoO_2$-coated $LiMn_2O_4$ samples was analyzed by inductively-coupled plasma emission spectrograph (ICP-ES).

For the electrochemical measurement, two-electrode cells were employed with lithium foils as the counter and reference electrodes. The working electrode was fabricated by mixing the prepared $LiMn_2O_4$, acetylene black, and PTFE latex with a mass ratio of 8:1:1. A slurry of the above mixture was dried in a vacuum oven at 120 °C, and then uniaxially pressed into a nickel mesh under a pressure of 30 MPa. 1 M lithium hexafluorophosphate ($LiPF_6$) solution in a mixture of ethylene carbonate (EC) and diethyl carbonate (DEC) with a volume ratio of 1:1 was used as the electrolyte. The lithium-ion cells were assembled in a glove box purged with floating argon. Electrochemical properties were investigated using the land battery measurement system (Wuhan, PR China). All the galvanostatic charge/discharge tests were performed at room temperature and cycled in the voltage range of 4.2–3.5 V at a current rate of 0.2 C.

3. Results and discussion

3.1. Characterization of the as-prepared MnO_2 spherical precursors

Fig. 1 shows the SEM images and EDX pattern of the prepared MnO_2 spherical precursors. Fig. 1a reveals that the prepared MnO_2 sample consists of spherical particles with coarse surfaces. The particle size of the MnO_2 sample ranges from 1 to 4 μm. Fig. 1b displays

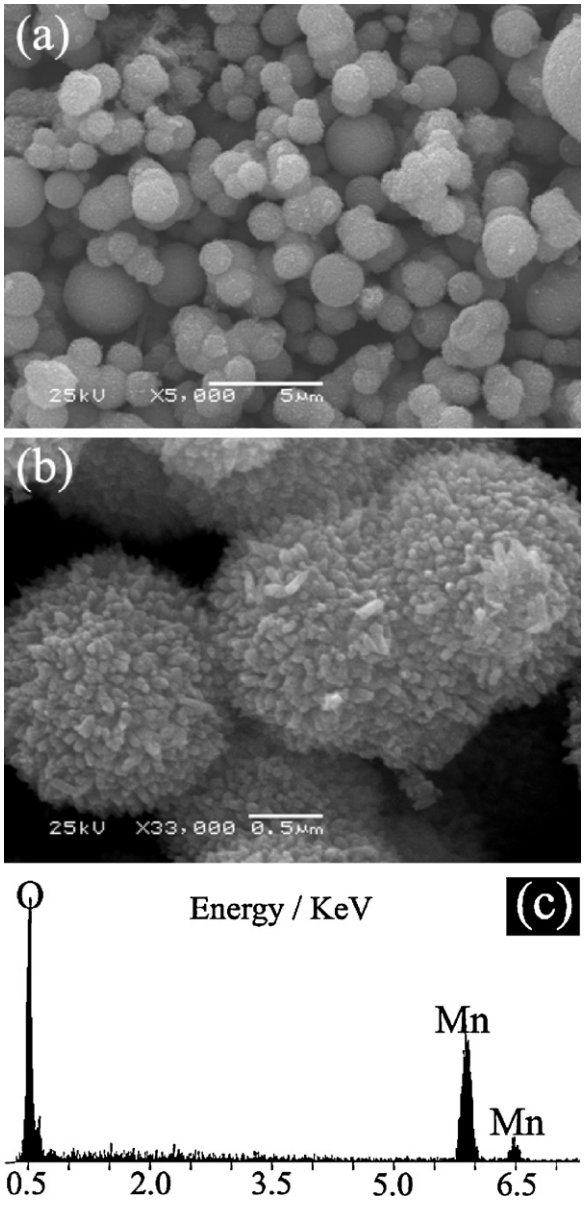

Fig. 1. SEM images and EDX pattern of the as-prepared MnO_2 spherical precursors.

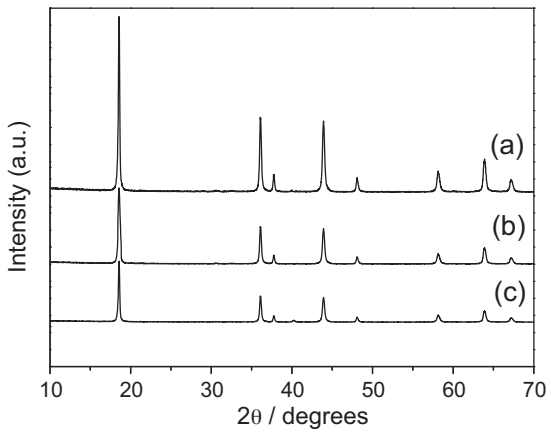

Fig. 2. XRD patterns of the as-prepared samples: (a) $LiMn_2O_4$ prepared by the hydrothermal reaction, (b) $LiMn_2O_4$ synthesized by the solid-state reaction, and (c) $LiCoO_2$-coated $LiMn_2O_4$ obtained by the sol–gel process.

the high-magnification SEM photograph of several MnO_2 spheres, which reveals that one-dimensional nanostructures are vertically grown on the surfaces of the MnO_2 spheres. Fig. 1c presents the EDX pattern of the prepared sample. From the EDX pattern, it is clear that only Mn and O elements with a molar ratio of ca. 1:2 exist in the sample, confirming that the prepared sample is MnO_2.

3.2. Phases and morphologies of the as-synthesized $LiMn_2O_4$ samples by different methods

Fig. 2a and b shows the XRD patterns of the $LiMn_2O_4$ samples synthesized by hydrothermal and solid-state reactions, respectively. All the diffraction peaks in Fig. 2a and b can be readily indexed to pure spinel $LiMn_2O_4$ with *Fd*3*m* space group (JCPDS card No. 35-0782). The sharp diffraction peaks indicate that the prepared $LiMn_2O_4$ samples are well crystalline. In addition, the much sharper reflection peaks in Fig. 2a suggest that the crystallinity of the $LiMn_2O_4$ synthesized by the hydrothermal route is higher than that prepared by the solid-state reaction. Fig. 2c shows the XRD pattern of the $LiCoO_2$-coated $LiMn_2O_4$ particles. It is found that all the reflection peaks can be indexed to pure spinel phase similar to Fig. 2a and b, suggesting that the small amount of surface coating of $LiCoO_2$ does not change the crystal structure of spinel $LiMn_2O_4$.

Fig. 3 shows the SEM micrographs of the $LiMn_2O_4$ sample synthesized by the hydrothermal reaction of MnO_2 spheres in LiOH aqueous solution. From Fig. 3a, it is seen that the resultant $LiMn_2O_4$ sample mainly consists of large quantities of particles with a size less than 1 μm. Fig. 3b gives a high-magnification image of several selected $LiMn_2O_4$ particles. It is found that the prepared $LiMn_2O_4$ sample is composed of particles with well-developed octahedral shapes (see the arrow) [13,14]. In addition, very few quasi-spherical particles can also be observed in Fig. 3c as indicated by the arrow. However, a high-magnification micrograph in Fig. 3d indicates the outer part of this quasi-spherical $LiMn_2O_4$ particle has been evolved to a lot of small polyhedral particles, suggesting that the spherical morphology of MnO_2 has been destroyed during the hydrothermal reaction of MnO_2 in LiOH solution.

Fig. 4 shows the SEM micrographs of the $LiMn_2O_4$ sample synthesized by the solid-state reaction of MnO_2 spheres and $LiOH{\cdot}H_2O$. From Fig. 4a, it is observed that the prepared $LiMn_2O_4$ sample is composed of a large quantity of microspheres with a size ranging from 1 to 8 μm in addition to few sintered aggregates. Fig. 4b presents a high-magnification SEM image of a single $LiMn_2O_4$ spherical particle. It indicates that its surface is constructed of large quantities of small rod-shaped particles. Fig. 4 demonstrates that the spherical morphology of MnO_2 has been well preserved during the calcination of the mixture of MnO_2 and $LiOH{\cdot}H_2O$.

In current experiments, it is noticed that the morphologies of $LiMn_2O_4$ products are very different when prepared by different

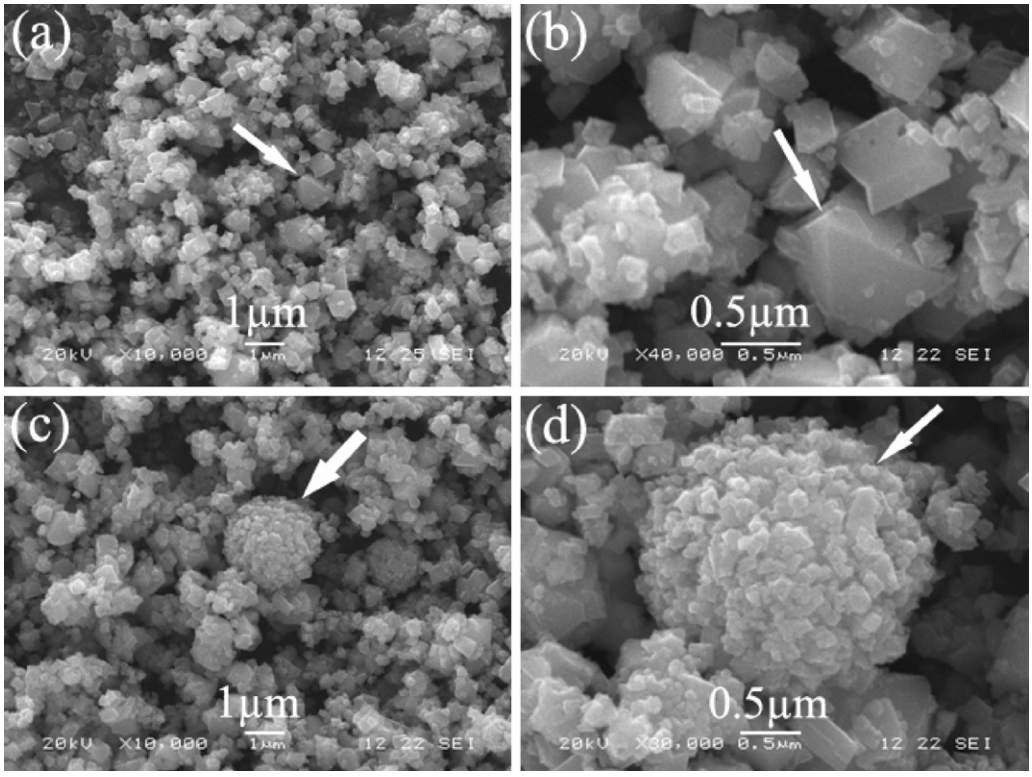

Fig. 3. SEM images of the $LiMn_2O_4$ octahedrons synthesized by the hydrothermal reaction.

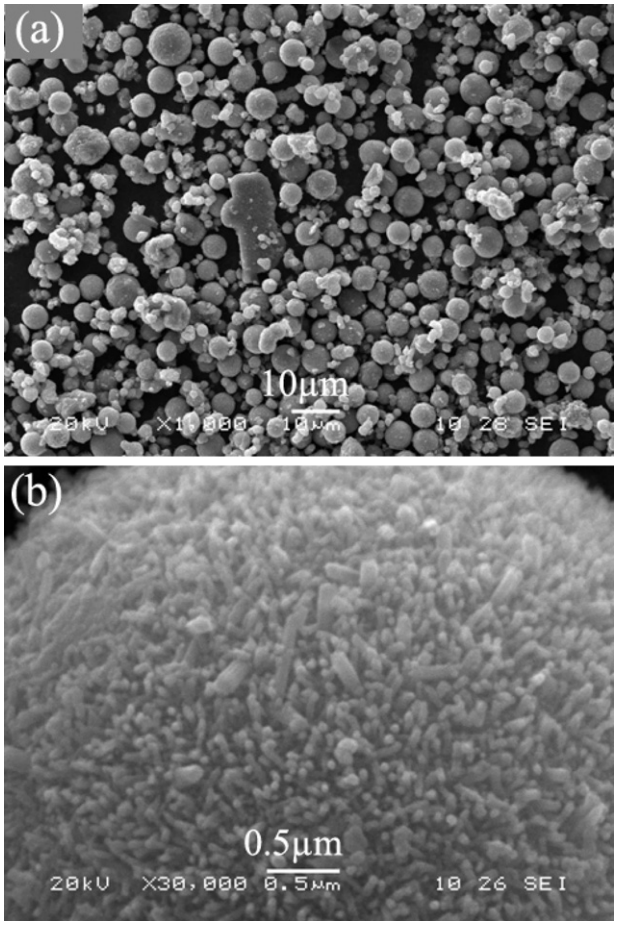

Fig. 4. SEM images of the $LiMn_2O_4$ microspheres synthesized by the solid-state reaction.

synthetic methods. We think this should be mainly caused by the different reaction environments involved.

In the synthesis of $LiMn_2O_4$ by the hydrothermal reaction of MnO_2 in LiOH solution, several processes may be involved. Recently, it has been reported [42–44] that MnO_2 nanowires can be directly obtained by hydrothermal treatment of commercial MnO_2 particles in neutral or alkaline solutions via a dissolution–recrystallization process. Likewise, it is worthy believing that the as-prepared MnO_2 spherical precursors in present experiments will also undergo a similar dissolution–recrystallization process during the hydrothermal treatment. That is, part of MnO_2 spheres would dissolve into the LiOH solution during the hydrothermal treatment. In addition, some MnO_2 molecules would be reduced by OH^- in the solution simultaneously to form MnOOH molecules along with the production of O_2 [43]. The resulting MnOOH thus can further react with LiOH and MnO_2 to form $LiMn_2O_4$ nuclei. Next, spinel $LiMn_2O_4$ microcrystals will be produced via the preferential growth of $LiMn_2O_4$ nuclei along its specific crystal facets. Finally, spinel $LiMn_2O_4$ octahedrons would be obtained as a result. The possible chemical reactions that occurred during the hydrothermal process can be formulated as follows:

$$[MnO_2]_n \rightarrow xMnO_2 + [MnO_2]_{(n-x)} \quad (1)$$

$$4MnO_2 + 2H_2O \rightarrow 4MnOOH + O_2\uparrow \quad (2)$$

$$LiOH + MnO_2 + MnOOH \rightarrow LiMn_2O_4 + H_2O \quad (3)$$

The overall reaction equation can thus be expressed as follows:

$$4LiOH + 8MnO_2 \rightarrow 4LiMn_2O_4 + 2H_2O + O_2\uparrow \quad (4)$$

In contrast, as to the preparation of $LiMn_2O_4$ by the solid-state reaction of MnO_2 and $LiOH{\cdot}H_2O$, the possible chemical reactions can be expressed in the following:

$$4MnO_2 \rightarrow 2Mn_2O_3 + O_2\uparrow \quad (5)$$

$$2LiOH{\cdot}H_2O + 2MnO_2 + Mn_2O_3 \rightarrow 2LiMn_2O_4 + 3H_2O\uparrow \quad (6)$$

The whole reaction equation can be formulated as:

$$4LiOH{\cdot}H_2O + 8MnO_2 \rightarrow 4LiMn_2O_4 + 6H_2O\uparrow + O_2\uparrow \quad (7)$$

That is, MnO_2 will firstly decompose to produce Mn_2O_3 and O_2 at elevated temperature of around 500 °C. Next, LiOH, MnO_2, and new-formed Mn_2O_3 can react under high calcination temperature to form spinel $LiMn_2O_4$ crystals, accompanied with the release of H_2O in the form of vapor. Compared with the hydrothermal process, the whole solid-state reaction takes place at a high-temperature gas–solid phase atmosphere, in which no dissolution–recrystallization process will be involved. In addition, it is also noted that spherical particles have the lowest surface energies during the calcination process. Hence, the morphology of MnO_2 precursors can be well preserved during the annealing process and copied to the resulting $LiMn_2O_4$ except for the increase of particle size due to the growth of crystal grains at high calcination temperature. Recently, $LiMn_2O_4$ nanorods have also been appropriately prepared by the solid-state reaction of MnO_2 nanorods and lithium salts [38,39], which further indicates that the solid-state reaction may be an appropriate route to synthesize spinel $LiMn_2O_4$ with desired morphology by selecting suitable manganese oxide precursors.

3.3. Characterization of the as-prepared $LiCoO_2$-coated $LiMn_2O_4$ microspheres

Fig. 5 shows the SEM images and EDX pattern of the $LiCoO_2$-coated $LiMn_2O_4$ sample synthesized by a sol–gel method. From Fig. 5a and b, it is found that the sample consists of a large quantity of spherical particles with a size range of 1–10 μm in addition to a few irregular agglomerates. Fig. 5c and d gives the microscopic morphologies of two individual $LiCoO_2$-coated $LiMn_2O_4$ spherical particles. It is observed that the surfaces of $LiMn_2O_4$ microspheres after coating with $LiCoO_2$ have become more smooth than that of pure $LiMn_2O_4$ microspheres synthesized by the solid-state reaction (Fig. 4b), suggesting that $LiCoO_2$ has been successfully coated on the $LiMn_2O_4$ microspheres. The EDX pattern of the $LiCoO_2$-coated $LiMn_2O_4$ microspheres is presented in Fig. 5e. From Fig. 5e, it is found that only Mn, O, and Co elements are detected in the EDX pattern. For the analysis of cobalt content in the final $LiCoO_2$-coated $LiMn_2O_4$ sample, ICP-ES analysis was performed. From the ICP analysis as shown in Table 1, it is seen that 3.2 mol% of cobalt was coated on the surface of $LiMn_2O_4$ microspheres.

3.4. Electrochemical properties of the as-prepared $LiMn_2O_4$ and $LiCoO_2$-Coated $LiMn_2O_4$ samples

Fig. 6 shows the initial charge–discharge curves and cycling properties of $LiMn_2O_4$ and $LiCoO_2$-coated $LiMn_2O_4$ samples. From Fig. 6, it is noted that all the three samples show two clear plateaus during the electrochemical charge–discharge processes, corresponding to the well-defined spinel $LiMn_2O_4$ materials, revealing that the surface coating of small amount of $LiCoO_2$ does not alter

Table 1
ICP analysis result of the $LiCoO_2$-coated $LiMn_2O_4$ sample.

Elements	Li	Mn	Co
Amount (mol%)	32.3	64.5	3.2

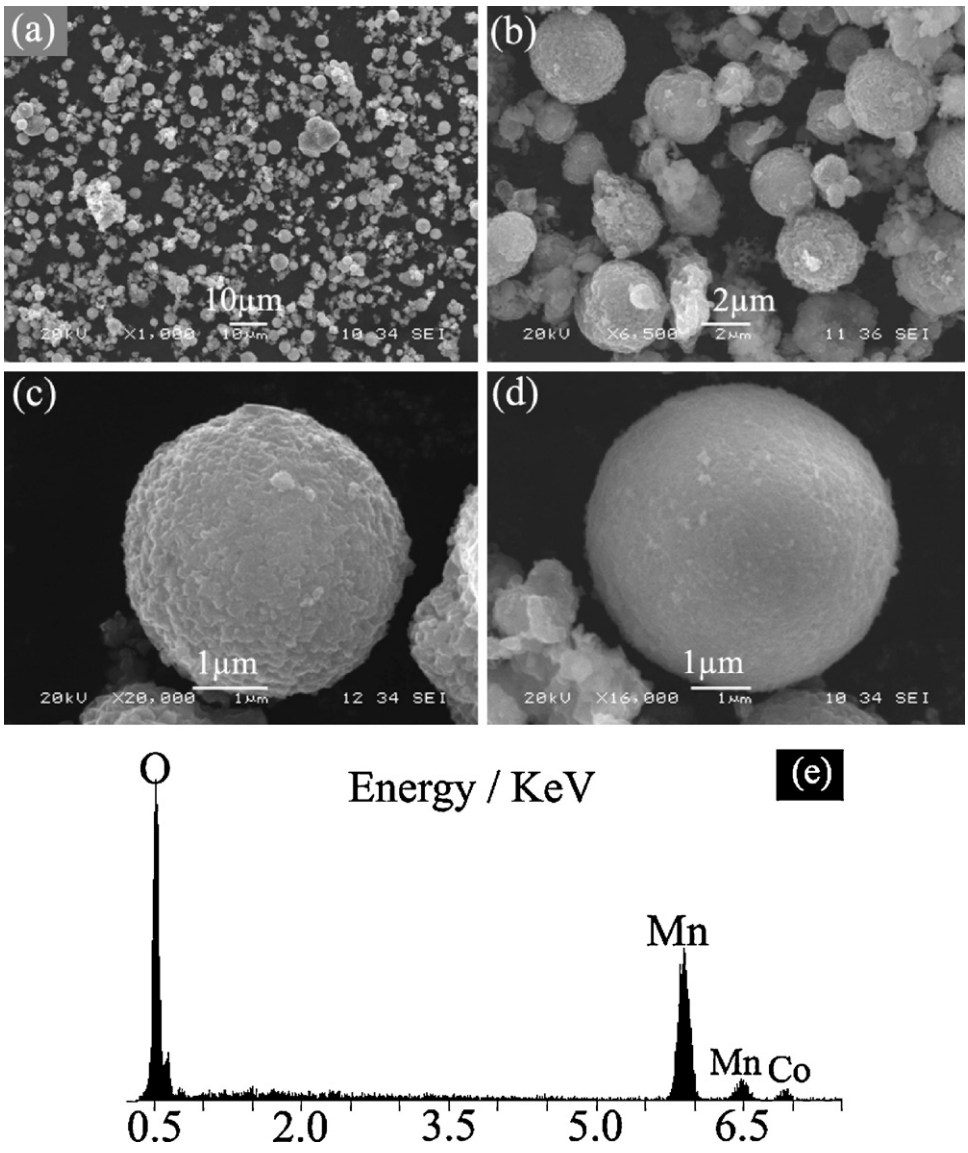

Fig. 5. SEM images and EDX pattern of the $LiCoO_2$-coated $LiMn_2O_4$ microspheres.

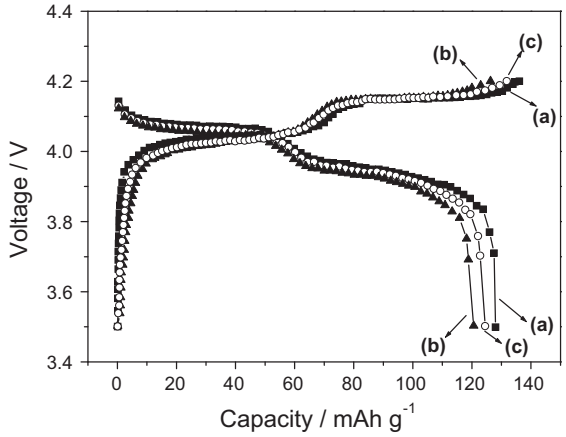

Fig. 6. First charge–discharge curves of the as-prepared samples: (a) $LiMn_2O_4$ octahedrons, (b) $LiMn_2O_4$ microspheres, and (c) $LiCoO_2$-coated $LiMn_2O_4$ microspheres.

the intrinsic electrochemical properties of $LiMn_2O_4$ as well as its spinel structure. The initial discharge capacity for the $LiMn_2O_4$ octahedrons (Fig. 6a) obtained by the hydrothermal reaction is 128 mAh g^{-1} while that of the $LiMn_2O_4$ microspheres (Fig. 6b) synthesized by the solid-state reaction is 120.6 mAh g^{-1}. The higher first discharge capacity of $LiMn_2O_4$ octahedrons may be due to the relatively high crystallinity and a small particle size compared to that of $LiMn_2O_4$ microspheres. After surface coating, the discharge capacity of the $LiCoO_2$-coated $LiMn_2O_4$ (Fig. 6c) increases to 124.5 mAh g^{-1}, which may be ascribed to the higher discharge capacity of $LiCoO_2$ compared to that of $LiMn_2O_4$. The cycling stability of the three electrodes is presented in Fig. 7. Obviously, the $LiMn_2O_4$ octahedrons exhibit a distinct discharge capacity loss during every charge–discharge cycle (Fig. 7a) compared to that of the $LiMn_2O_4$ microspheres (Fig. 7b). After being cycled for 50 times, the discharge capacity of the $LiMn_2O_4$ octahedrons retains 114.4 mAh g^{-1}, which is slightly higher than that of the $LiMn_2O_4$ microspheres (112.5 mAh g^{-1}). The capacity retentions of the $LiMn_2O_4$ octahedrons and $LiMn_2O_4$ microspheres are 89.4% and 93.3%, respectively. The better cycling properties of the $LiMn_2O_4$ microspheres may be attributed to the fact that the larger spherical particles can reduce the contact interface of electrode with electrolytes, resulting in the reduction of dissolution

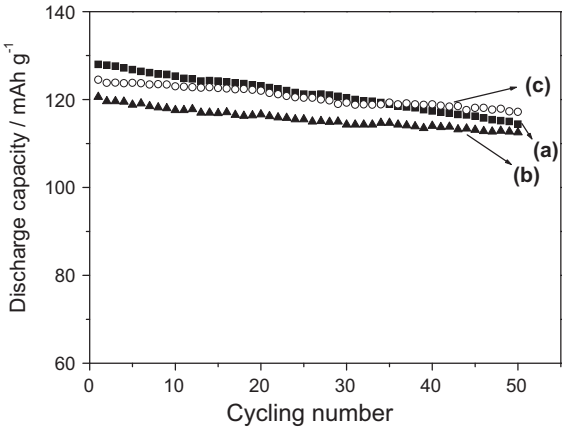

Fig. 7. Cycling properties of the as-prepared samples: (a) $LiMn_2O_4$ octahedrons, (b) $LiMn_2O_4$ microspheres, and (c) $LiCoO_2$-coated $LiMn_2O_4$ microspheres.

of Mn ions into the electrolyte during the electrochemical reactions. After surface modification, as shown in Fig. 7c, the $LiCoO_2$-coated $LiMn_2O_4$ electrode shows even superior cycle characteristics. The discharge capacity of the $LiCoO_2$-coated $LiMn_2O_4$ retains 117.2 mAh g^{-1}, with a capacity retention of 94.1%. This result indicates that the surface coating of appropriate amount of $LiCoO_2$ can both increase the discharge capacity and improve the cycle properties of the spinel $LiMn_2O_4$.

4. Conclusions

Spinel $LiMn_2O_4$ materials with different morphologies have been synthesized by two different methods with pre-prepared spherical MnO_2 particles as precursors. The $LiMn_2O_4$ sample obtained by the hydrothermal reaction mainly consists of large quantities of octahedral particles with a size less than 1 μm while the $LiMn_2O_4$ product prepared by the solid-state reaction is composed of microspheres with a size ranging from 1 to 8 μm. The morphology difference should be ascribed to the different reaction processes involved under different reaction conditions. Moreover, $LiCoO_2$ was coated on the surface of $LiMn_2O_4$ microspheres by a sol–gel route. Electrochemical measurements indicate that the as-synthesized $LiMn_2O_4$ octahedrons have a higher initial discharge capacity (128 mAh g^{-1}) compared to that of the as-prepared $LiMn_2O_4$ microspheres (120.6 mAh g^{-1}) and $LiCoO_2$-coated $LiMn_2O_4$ (124.5 mAh g^{-1}). However, $LiMn_2O_4$ microspheres and $LiCoO_2$-coated $LiMn_2O_4$ microspheres display much superior capacity retentions than that of $LiMn_2O_4$ octahedrons. After cycling for 50 times, the capacity retentions of the $LiMn_2O_4$ octahedrons, $LiMn_2O_4$ microspheres, and $LiCoO_2$-coated $LiMn_2O_4$ microspheres are 89.4%, 93.3%, 94.1%, respectively. The synthetic method for the preparation of $LiMn_2O_4$ microspheres by the solid-state reaction presented here can be potentially developed to synthesize other Li–Mn–O oxides and metal-doped spinel $LiMn_2O_4$ with fine electrochemical properties by controlling appropriate stoichiometry ratio of the initial precursors and optimizing experimental parameters.

Acknowledgments

This work was financially supported by Provincial Natural Science Foundation of Hunan (No. 09JJ3024) and the opening subject of State Key Laboratory of Powder Metallurgy (No. 2008112032).

References

[1] J.M. Tarascon, E. Wang, F.K. Shokoohi, W.R. Mckinnon, S. Colson, J. Electrochem. Soc. 138 (1991) 2859–2864.
[2] J.M. Tarascon, M. Armand, Nature 414 (2001) 359–367.
[3] C.H. Lu, S.W. Lin, J. Power Sources 97–98 (2001) 458–460.
[4] J.H. Choy, D.H. Kim, C.W. Kwon, S.J. Hwang, Y.I. Kim, J. Power Sources 77 (1999) 1–11.
[5] K. Matsuda, I. Taniguchi, J. Power Sources 132 (2004) 156–160.
[6] H. Huang, C.H. Chen, R.C. Perego, E.M. Kelder, L. Chen, J. Schoonman, W.J. Weydanz, D.W. Nielsen, Solid State Ionics 127 (2000) 31–42.
[7] C. Wan, Y. Nuli, J. Zhuang, Z. Jiang, Mater. Lett. 56 (2002) 357–363.
[8] S.H. Ye, J.Y. Lv, X.P. Gao, F. Wu, D.Y. Song, Electrochim. Acta 49 (2004) 1623–1628.
[9] X. Qiu, X. Sun, W. Shen, N. Chen, Solid State Ionics 93 (1997) 335–339.
[10] K.T. Hwang, W.S. Um, H.S. Lee, J.K. Song, K.W. Chung, J. Power Sources 74 (1998) 169–174.
[11] C.H. Lu, S.K. Saha, Mater. Sci. Eng. B: Solid 79 (2001) 247–250.
[12] W. Liu, K. Kowal, G.C. Farrington, J. Electrochem. Soc. 143 (1996) 3590–3596.
[13] H.M. Wu, J.P. Tu, Y.F. Yuan, X.T. Chen, J.Y. Xiang, X.B. Zhao, G.S. Cao, J. Power Sources 161 (2006) 1260–1263.
[14] C.H. Jiang, S.X. Dou, H.K. Liu, M. Ichihara, H.S. Zhou, J. Power Sources 172 (2007) 410–415.
[15] M.M. Thackeray, Prog. Solid State Chem. 25 (1997) 1–71.
[16] G.G. Amatucci, C.N. Schmutz, A. Blyr, C. Sigala, A.S. Gozdz, D. Larcher, J.M. Tarascon, J. Power Sources 69 (1997) 11–25.
[17] Y. Xia, M. Yoshio, J. Power Sources 66 (1997) 129–133.
[18] M. Hosoya, H. Ikuta, M. Wakihara, Solid State Ionics 111 (1998) 153–159.
[19] Y.K. Sun, D.W. Kim, Y.M. Choi, J. Power Sources 79 (1999) 231–237.
[20] G.T.K. Fey, C.Z. Lu, T.P. Kumar, Mater. Chem. Phys. 80 (2003) 309–318.
[21] K. Dokko, S. Horikoshi, T. Itoh, M. Nishizawa, M. Mohamedi, I. Uchida, J. Power Sources 90 (2000) 109–115.
[22] R. Singhal, S.R. Das, M.S. Tomar, O. Ovideo, S. Nieto, R.E. Melgarejo, R.S. Katiyar, J. Power Sources 164 (2007) 857–861.
[23] S.C. Park, Y.M. Kim, Y.M. Kang, K.T. Kim, P.S. Lee, J.Y. Lee, J. Power Sources 103 (2001) 86–92.
[24] Z. Liu, H. Wang, L. Fang, J.Y. Lee, L.M. Gan, J. Power Sources 104 (2002) 101–107.
[25] J. Tu, X.B. Zhao, G.S. Cao, D.G. Zhuang, T.J. Zhu, J.P. Tu, Eletrochim. Acta 51 (2006) 6456–6462.
[26] L. Yu, X. Qiu, J. Xi, W. Zhu, L. Chen, Eletrochim. Acta 51 (2006) 6406–6411.
[27] H. Liu, C. Cheng, Q. Zong, K. Zhang, Mater. Chem. Phys. 101 (2007) 276–279.
[28] J. Tu, X.B. Zhao, J. Xie, G.S. Cao, D.G. Zhuang, T.J. Zhu, J.P. Tu, J. Alloys Compd. 432 (2007) 313–317.
[29] D. Liu, Z. He, X. Liu, Mater. Lett. 61 (2007) 4703–4706.
[30] H.W. Ha, N.J. Yun, K. Kim, Electrochim. Acta 52 (2007) 3236–3241.
[31] D.Q. Liu, X.Q. Liu, Z.Z. He, Mater. Chem. Phys. 105 (2007) 362–366.
[32] S. Lim, J. Cho, Electrochem. Commun. 10 (2008) 1478–1481.
[33] H. Şahan, H. Göktepe, Ş. Patat, A. Ülgen, Solid State Ionics 178 (2008) 1837–1842.
[34] X.M. He, J.J. Li, Y. Cai, Y. Wang, J. Ying, C. Jiang, C. Wan, J. Solid State Electrochem. 9 (2005) 438–444.
[35] S.W. Oh, S.H. Park, K. Amine, Y.K. Sun, J. Power Sources 160 (2006) 558–562.
[36] M.H. Kim, H.S. Shin, D. Shin, Y.K. Sun, J. Power Sources 159 (2006) 1328–1333.
[37] I. Taniguchi, N. Fukuda, M. Konarova, Powder Technol. 181 (2008) 228–236.
[38] H. Fang, L. Li, Y. Yang, G. Yan, G. Li, J. Power Sources 184 (2008) 494–497.
[39] D.K. Kim, P. Muralidharan, H.W. Lee, R. Ruffo, Y. Yang, C.K. Chan, H. Peng, R.A. Huggins, Y. Cui, Nano Lett. 8 (2008) 3948–3952.
[40] H. Wang, D. Qian, Z. Lu, Y. Li, R. Cheng, Y. Li, J. Phys. Chem. Solids 68 (2007) 1422–1427.
[41] H.E. Wang, Z. Lu, D. Qian, S. Fang, J. Zhang, J. Alloys Compd. 466 (2008) 250–257.
[42] Z.Y. Yuan, Z. Zhang, G. Du, T.Z. Ren, B.L. Su, Chem. Phys. Lett. 378 (2003) 349–353.
[43] M. Wei, Y. Konishi, H. Zhou, H. Sugihara, H. Arakawa, Nanotechnology 16 (2005) 245–249.
[44] G. Li, L. Jiang, H. Pang, H. Peng, Mater. Lett. 61 (2007) 3319–3322.